

Electrochemical Analysis of the Corrosion Behavior of Drill Pipe Steel under Oil/Water Emulsion Condition

Yisheng Hu^{1,2*}, Yu Peng¹, Jinzhou Zhao¹, Ping Guo¹, Siping Long³

¹ State Key Laboratory of Oil and Gas Reservoir Geology and Exploitation, Southwest Petroleum University, Chengdu, 610500, China

² Department of Earth Science and Engineering, Imperial College London, London, SW7 2AZ, UK

³ Sichuan Geophysical Company, CNPC, Chengdu, 610213, China

*E-mail: huyisheng008@yahoo.com

Received: 21 May 2017 / *Accepted:* 19 June 2017 / *Published:* 13 August 2017

This work proposed a rotating disk electrode strategy to study the electrochemical corrosion performance of API-X100 pipeline steel immersed in a simulated oil/water emulsion under controlled electrochemical and hydrodynamic conditions. The mass-transfer of oxygen was found to be crucial to the cathodic process of steel in solution both before and after the addition of oil. Electrode rotation sped up the cathodic reduction by accelerating oxygen diffusion. In the solution, after the addition of oil, there was an increment in the limiting diffusive current density (LDCD), which resulted from the enhanced solubility of oxygen in the oil/water emulsion. The anodic current density decrease caused by the electrode rotating speed (ERS) increment resulted from the accelerated oxygen diffusion and reduction along with the enhancement in the oxidation of the steel. With the addition of oil, the anodic dissolution of steel decreased. This phenomenon was ascribed to the fact that a layer of an oily phase formed on the surface of the steel and the reaction activation energy increased. Upon the addition of oil, a variation of the corrosion reaction mechanism was observed, indicating the activation-controlled feature of the interfacial reaction instead of the mass-transfer controlled property.

Keywords: Corrosion behavior; Electrochemical analysis; Drill pipe steel; Oil/water emulsion

1. INTRODUCTION

Non-traditional oil production, including from Canadian oil sands [1, 2], has been accepted as a crucial way of catering to the ever-increasing requirement for energy consumption. The oil sands are developed into an oil sand slurry after being mixed with warm water. This slurry is subsequently delivered to the extraction plant via pipelines for further processing. Hydro-transportation is

acknowledged as a flexible and economic technique for oil sands transportation [3]. Nevertheless, corrosion and erosion–corrosion pose a primary risk to the integrity of a hydro-transport system [4-7].

The combination of oxygen, water, and varying salts, including Cl^- and HCO_3^- , along with the elevated content of sand particles, in the oil sands slurry lead to pipe steel corrosion, and erosion speeds up through the flowing slurry [8]. Compared with the single use of erosion or corrosion, their synergistic effects cause significant material loss [9-16].

Studies on the corrosion of hydro-transport pipe steel immersed in oil sands slurry were considered sophisticated due to the synergistic effects of operating parameters and the varying components of steel corrosion. For instance, a layer of oily phase formed over the surface of the steel, which led to decreased steel corrosion; hence, a great alteration in the corrosion performance of the steel resulted from the destabilization of the emulsion [17-25]. Huet and co-workers [26, 27] proposed that the steel corrosion and electrolyte resistance of the steel fluctuate due to the variation in oil/brine composition near the electrode surface. In addition, sand particle impingement and the hydrodynamic condition of the slurry were believed to initially affect the coverage of the oily phase and subsequently the steel corrosion performance.

Despite the extensive used of emulsions, the electrochemical and corrosion performance of metals in emulsified systems has received little concern. Studies on the electrochemical performance of metallic surfaces in emulsions under controlled hydrodynamic conditions will help better understand the effect that the oily phase has on corrosion. This work studied the electrochemical performance of API-X100 pipeline steel immersed in oil-in-water emulsions under controlled electrochemical and hydrodynamic conditions to investigate the relationship among the electrochemical technique–determined corrosion rate, hydrodynamic conditions and oil content of this emulsion. The results obtained in these studies are crucial for understanding the importance that oil has in modifying the rate and mechanism of corrosion.

2. EXPERIMENTS

2.1. Oil/water emulsions

NaHCO_3 (0.02 M) and NaCl (0.02 M) were mixed using 0.2 wt% dioctyl sulfosuccinate sodium salt to form the anionic surfactant agent. The oil–water emulsion consisted of 20[#] engine oil (1 g/L), Tween 80 (0.5 g/L), Span 80 (0.5 g/L) and distilled water. This agent served as the basic experimental solution and was used to achieve a uniform mixing of oil in the emulsion. This basic solution was mixed with a light mineral oil of varying concentrations (density: 0.90 g/cm^3) to synthesize the oil/water emulsions. The oil sands slurry was simulated by adding sand particles (10 wt%; average size: 100 μm ; Lane Mountain products) to the as-prepared oil/water emulsion. The pH values of solutions with and without 10% oily phase were 8.62 and 8.57, respectively. A particle size analyzer was used to determine the average drop size. In all cases, the drop size exhibited a unimodal distribution, averaged as 11 μm .

2.2. API-X100 carbon steel

The experimental specimens were cut from an API-X100 steel-made oil pipeline. The chemical composition and carbon equivalent of this steel are recorded (Table 1). There were two polishing process prior to each test, initially with SiC paper to 1200 grit and then with Al₂O₃ powder (0.05 μm) to a mirror-like finish.

Table 1. The chemical composition and carbon equivalent of the API-X100 steel.

Composition (wt. %)									
C	Mn	Mo	Ni	Al	Cu	Ti	Nb	Cr	V
0.1	1.65	0.18	0.13	0.02	0.24	0.03	0.042	0.016	0.003

2.3. Experimental apparatus

The rotating disk electrode (RDE) (diameter: 0.5 cm) was used. The counter electrode formed by a serpentine platinum wire was protected using a porous membrane. The reference electrode was prepared by coupling a standard saturated calomel electrode (SCE) with a Luggin probe. The tip of this SCE was between the counter and working electrodes. The location of either the counter electrode or reference electrodes was arranged to avoid affecting the flow lines of the emulsion from/to the working electrode. The RDE rotated in a range (0 - 2500 rpm), whereas 800 rpm was applied in most of the tests. When the rotation rates exceeded 800 rpm, the main effects of the rotation rate could not be monitored in the electrochemical activity. Becerra and co-workers [22] proposed the utility of the jet impingement electrochemical cell in the test.

The morphology of the steel was observed by scanning electron microscopic (SEM) (JSM-6700F, JEOL). Electrochemical measurements were carried out using a Solartron 1280C electrochemical measurement configuration. The polarization profiles were plotted using different potentials in a range of -1.0 V to 2.0 V (*vs.* SCE), and the sweep rate was 1 mV/s. Further, the open circuit potential (OCP) was recorded for 300 s prior to each test. Electrochemical impedance assays were carried out at the corrosion potential, and the voltage perturbation amplitude was 20 mV, whereas the frequency fell in a range (10 kHz - 100 mHz). The specimens were left at the OCP for 300 s and were subsequently exposed to polarization at -1.0 V (*vs.* SCE) for 300 s, followed by measurement of the impedance at the pre-determined OCP, to standardize the sample surface.

3. RESULTS AND DISCUSSION

Figure 1 displays the microstructural properties investigated using scanning electron microscopy. Acicular ferrite and bainite colonies were found and are characteristic of a sophisticated microstructure, and the color showed slight variations, possibly due to local changes in the chemical composition.

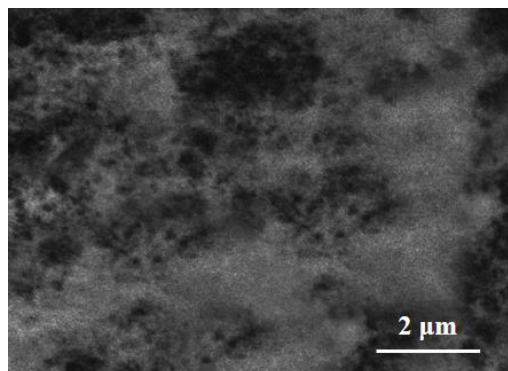


Figure 1. SEM pattern of API-X100 steel showing martensite (dark), bainite, and ferrite (light) colonies.

API-X100 steel in the presence and absence of oil (10 wt%) at varying electrodes was characterized via the cathodic polarization patterns shown in Figure 2. These two solutions showed a limiting current density (LCD) that increased markedly as the ERS increased. In addition, this figure shows a positive shift in the corrosion potential as the rotating speed increased. There was no limiting current phenomenon in the polarization of the electrode at high cathodic over-potentials, and the cathodic current density was found to be ERS-independent. Further, compared with the cathodic current density recorded at individual rotation speeds in solution before oil addition, that obtained in the oil/water emulsion was slightly elevated (Figure 1A and B). Upon electrode rotation, oxygen diffusion is accelerated, as is the cathodic reduction of oxygen [28]. Therefore, the cathodic current density and limiting diffusive current density increased with the increasing rotation speed, as shown in Figure 1. The oxygen reduction dominated the cathodic reaction of API-X100 steel in aerated aqueous solution before and after adding oil. The reduction process was described as follows:



The solution-dissolved oxygen molecules reached the surface of the steel after diffusing through the solution boundary layer before the reduction process occurred at the surface of the steel electrode. Therefore, cathodic polarization patterns displayed a LDCD due to the significant effect of the entire steel corrosion by the mass-transfer process.

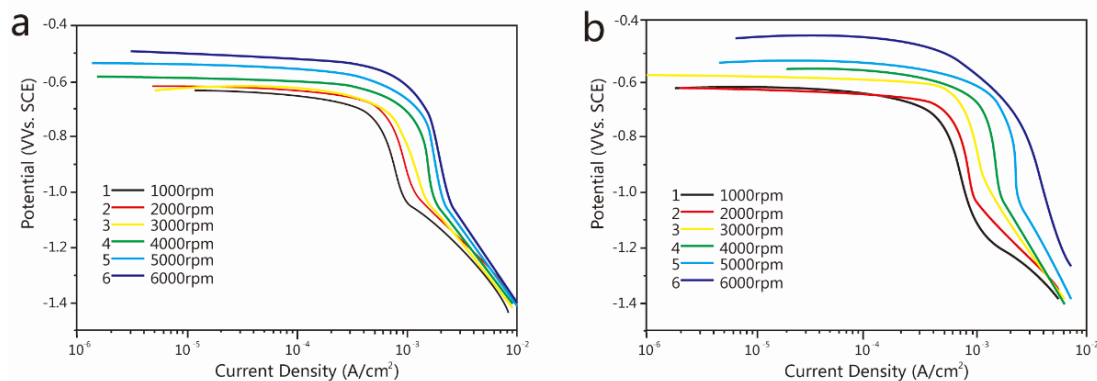
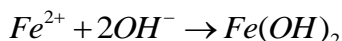


Figure 2. Cathodic polarization patterns of API-X100 steel in solutions (A) in the absence of and (B) in the presence of oil (10%) at 60 °C as a function of ERS.

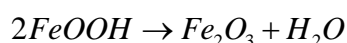
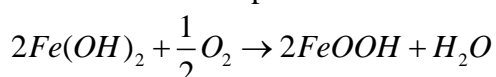
As indicated in Figure 3, the API-X100 steel in solutions before and after adding oil (10%) at varying electrodes was characterized via the anodic polarization patterns. As the ERS increased, the anodic current density was found to decrease in two cases, and a positive shift of the corrosion potential was observed. Further, the anodic current density obtained at the individual ERS decreased after adding oil. Iron dissolution characterized the anodic process of API-X100 steel in oil-free and oil-containing solutions:



where iron ions combined with hydroxide ions to form corrosion scale, $Fe(OH)_2$:



where the process began with the oxidization of $Fe(OH)_2$ into $FeOOH$ that was not stable and further oxidized to Fe_2O_3 after adding oxygen. Hence, Fe_2O_3 and $FeOOH$ were expected to be contained in the corrosion product.



For the two solutions before and after adding oil, as the ERS increased, the anodic current density was found to decrease, and a positive shift in the corrosion potential was observed (Figure 3). This phenomenon resulted from and promoted the production of $Fe(OH)_2$ scale and Fe_2O_3 film on the electrode surface. This promotion lay in the fact that the oxygen diffusion to the electrode surface for the reduction reaction had been sped up. The addition of oil also decreases the anodic dissolution of steel due to the formation of a layer of oily phase on steel surface, which inhibited the dissolution of steel [22].

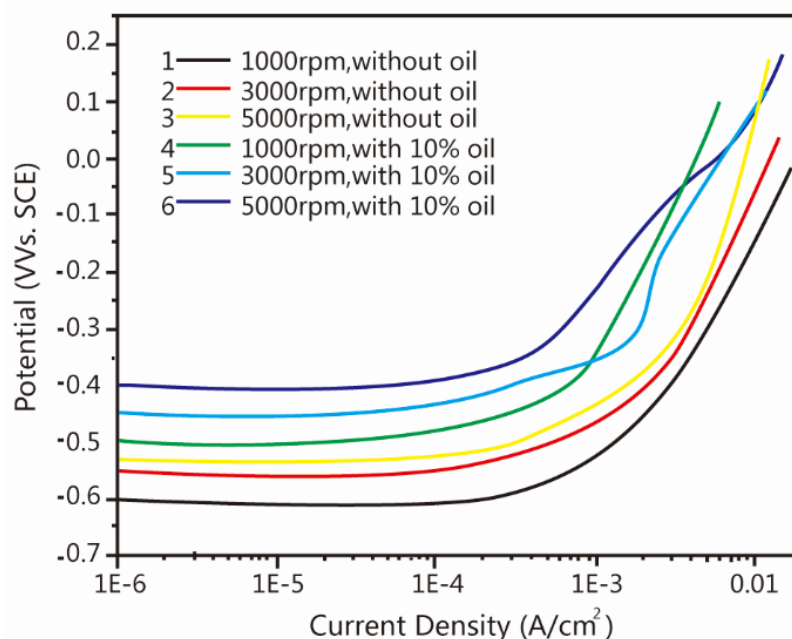


Figure 3. Anodic polarization patterns of API-X100 steel in solutions before and after adding oil (10 wt%) as a function of ERS.

API-X100 steel in solutions before and after adding oil (10 wt%) at varying temperatures (ERS: 3000 rpm) was characterized via the polarization patterns shown in Figure 4. As the temperature increased, there was an enhancement in the anodic dissolution current density, and a simultaneous negative shift of the corrosion potential of the steel was observed. The acceleration of the oxygen diffusion at elevated temperatures led to the formation of a protective corrosion scale, which resulted in decreased steel dissolution (Figure 4). However, this phenomenon was inadequate to offset the effect caused by the increment in interfacial dissolution. The pronounced anodic dissolution increase and a negative shift in corrosion potential suggested an enhanced activity of the steel electrode at higher temperatures. In addition, as the temperature increased, there was a sharp increase in the anodic current density of the steel, indicating a slight possibility that a less porous Fe_3O_4 would form on the electrode surface within the temperature range used. In fact, a further increase in the tested temperature could lead to the formation of Fe_3O_4 .

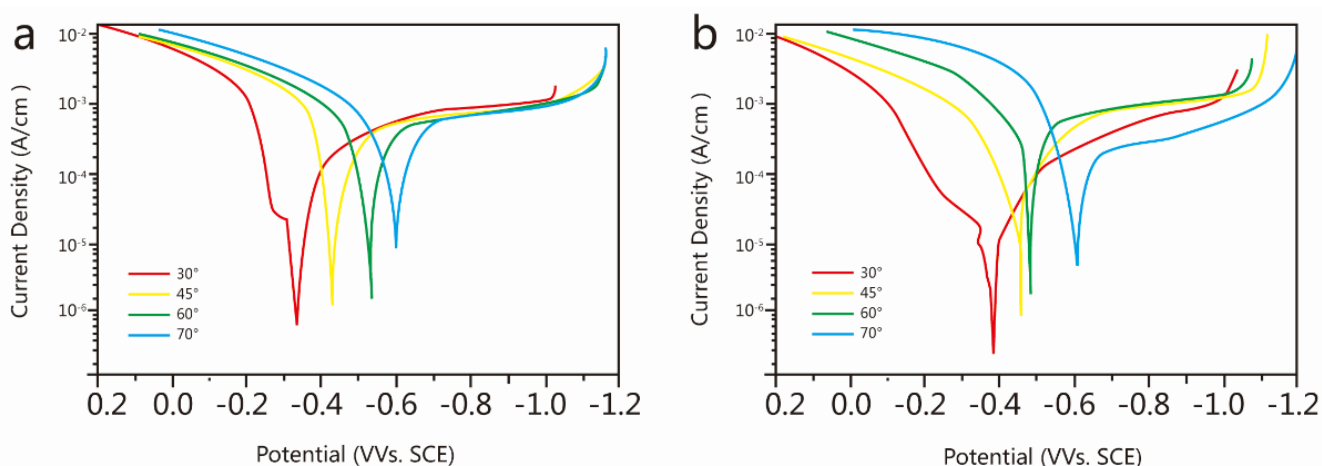


Figure 4. Polarization patterns of API-X100 steel in solutions in the (A) absence and (B) presence of oil (10%) (rotation speed: 3000 rpm) as a function of temperature.

API-X100 steel in varying concentrations of solutions at 60 °C (ERS: 3000 rpm) was displayed via Nyquist diagrams in Figure 5A. A capacitive semicircle at high frequency and a diffusive tail at low frequency were observed in the Nyquist profile in the oil-free solution. A variation in the EIS characterization after adding oil was observed. Simultaneously, the semicircle extension to the entire frequency range was observed. As the oil concentration increased, an increase in the semicircle size was observed. As shown in Figure 5B, the Nyquist plots of API-X100 steel were recorded at 60 °C (ERS: 3000 rpm) in the original solution, oil/water emulsion and oil/water/sand slurry. The diameter of the capacitive semicircle showed an obvious decrease after adding sand. Nevertheless, the impedance obtained with and without the addition of sand showed no variations. The Nyquist diagrams of API-X100 steel in oil/water emulsion at 60 °C (ERS: 1000 rpm) are shown in Figure 5C as a function of experimental time. For all characterizations, an extended semicircle over the test frequency range and an increase in semicircle diameter due to the increased immersion time could be observed.

Diffusive impedance was observed in the low-frequency range in oil-free solutions, as shown in the EIS characterization. This phenomenon resulted from the oxygen diffusion-controlled reaction process. The variation in the EIS characteristics after adding oil to the solution indicated the variation in the corrosion reaction mechanism. A capacitive semicircle was recorded over the entire frequency range, suggesting the activation-controlled property of the interfacial reaction. A layer of oily phase formed, which inhibited the interfacial electron-transfer reaction instead of the mass-transfer step. The obvious decrease in charge-transfer resistance upon the addition of sand particles to the oil/water emulsion suggested that the corrosion of steel significantly increased. The sands in the flowing slurry could affect and even damage the oily and oxide films produced on the steel surface, ultimately leading the bare steel to be exposed to the corrosive solution. In addition, the sand particle-induced effect led to a rougher electrode surface, corresponding to an increased number of depressed semicircles over that of the solution without sand.

Table 2. EIS parameters recorded at 60 °C in solutions before and after oil addition (rotating speed: 3000 rpm).

Solution	D_O (cm ² /s)	ν (cm ² /s)	C_O (mol/L)	k_m (cm/s)	i_K (-0.7V) (mA/cm ²)	i_K (-0.9 V) (mA/cm ²)
0% oil	2.24×10^{-5}	0.011	7.71×10^{-4}	0.018	0.142	0.181
10% oil	1.74×10^{-4}	0.013	2.24×10^{-3}	0.016	0.155	0.245

The Reynolds numbers (the ratio of inertial forces to viscous forces within a fluid that is subjected to relative internal movement due to different fluid velocities) of the test system obtained in this test range from 250 to 3400. It is typically a laminar flow condition, compared to a transition Re of 2×10^5 to turbulent flow [29]. Based on the Levich equation, a diffusion-controlled electrode process on RDE under laminar flow conditions could be described as follows:

$$i_L = 0.62nFAD_o^{2/3} \omega^{1/2} \nu^{-1/6} C_O$$

where i_L represents the steady-state LDCD, n means the electron transfer number during the redox process, F represents Faraday's constant, A represents electrode area, D_O represents the diffusion coefficient of oxygen, ω represents the angular rotating velocity of the RDE, ν represents the kinematics viscosity, and C_O represents the concentration of oxygen. The steady-state LDCD was found to be linearly related to the square root of angular velocity, $\omega^{1/2}$. Apparently, the Levich law is followed strictly in both oil-free and oil-containing solutions. In the case of an unknown oxygen diffusion coefficient, the slope of the lines could be used to determine the concentrations of dissolved oxygen in oil-free and oil-containing solutions.

$$D_o = 6.92 \times 10^{-10} \left(\frac{T}{\nu} \right)$$

Varying kinetic parameters such as the fitted oxygen concentrations and diffusion coefficients of oxygen were recorded for solutions before and after adding oil (10%) in Table 2. D_o is the diffusion coefficient of oxygen; v is the oxygen concentration; C_o is the oxygen concentration; k_m is the mass-transfer coefficient; and i_k is the kinetic current density. Compared with the water, the oxygen concentration in the oil/water emulsion was approximately two times higher. Hence, the increased solubility of oxygen in solution after adding oil led to the increment of cathodic current density in oil/water emulsion. In fact, previous work [30, 31] has confirmed that there is a higher solubility of oxygen in the oil/water mixture than in pure water.

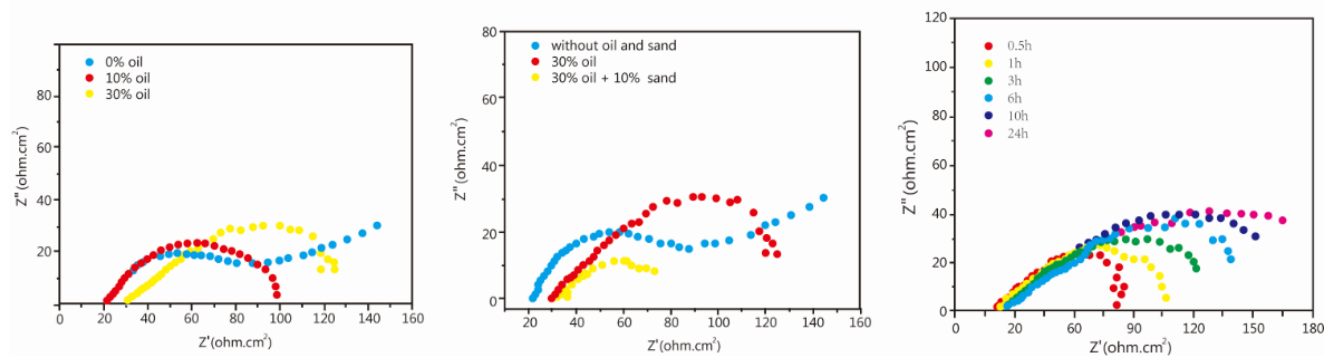


Figure 5. Nyquist patterns of API-X100 steel in (A) solutions before and after adding oil with varying concentrations at 60 °C (ERS: 3000 rpm), (B) solutions before and after adding sands (10%) or oil (30%) at 60 °C (ERS: 3000 rpm) and (C) in solution with oil (10%) at 60 °C (ERS: 1000 rpm) as a function of immersion time.

4. CONCLUSIONS

In summary, the mass-transfer of oxygen has been found to be crucial in the cathodic process of API-X100 pipe steel in the solution before and after adding oil. The electrode rotation sped up the cathodic reduction by accelerating oxygen diffusion. The enhanced solubility of oxygen in the oil/water emulsion led to an increase in the LDCD obtained in the oil-containing solution. For the solution before and after adding oil, as the ERS increased, a decrease in the anodic current density was observed. This phenomenon resulted from an enhancement in steel oxidation due to the acceleration of oxygen diffusion to the electrode surface for the reduction reaction. In the absence of oil, the corrosion of steel is an oxygen diffusion-controlled process. The varied EIS characterization after adding oil indicated a variation in the corrosion reaction mechanism and the activation-controlled property of the interfacial reaction.

References

1. F. Eliyan, E. Mahdi and A. Alfantazi, *Corrosion Science*, 58 (2012) 181.
2. G. Zhang and Y. Cheng, *Corrosion Science*, 51 (2009) 87.
3. P. Okafor, X. Liu and Y. Zheng, *Corrosion Science*, 51 (2009) 761.

4. O. Ouachikh, A. Bouyanzer, M. Bouklah, J. Desjobert, J. Costa, B. Hammouti and L. Majidi, *Surface Review and Letters*, 16 (2009) 49.
5. H. Ma and B. Wang, *J. Hazard. Mater.*, 132 (2006) 237.
6. L. Bammou, B. Chebli, R. Salghi, L. Bazzi, B. Hammouti, M. Mihit and H. Idrissi, *Green. Chem. Lett. Rew.*, 3 (2010) 173.
7. N. Lahhit, A. Bouyanzer, J.M. Desjobert, B. Hammouti, R. Salghi, J. Costa, C. Jama, F. Bentiss and L. Majidi, *Portugaliae Electrochimica Acta*, 29 (2011) 127.
8. D.B. Hmamou, R. Salghi, A. Zarrouk, B. Hammouti, S.S. Al-Deyab, H. Zarrok, A. Chakir, L. Bammou and L. Bazzi, *Int. J. Electrochem. Sci.*, 7 (2012) 2361.
9. M. Znini, L. Majidi, A. Bouyanzer, J. Paolini, J. Desjobert, J. Costa and B. Hammouti, *Arabian Journal of Chemistry*, 5 (2012) 467.
10. L. Afia, R. Salghi, L. Bammou, E. Bazzi, B. Hammouti, L. Bazzi and A. Bouyanzer, *Journal of Saudi Chemical Society*, 18 (2014) 19.
11. E. Kryzhaniv's'kyi and H. Nykyforchyn, *Materials Science*, 47 (2011) 127.
12. M. Setoudeh, A. Samimi, S. Zarinabadi, B. Almasinia, E. Nazem, R. Rezaei and A. Hedayati, *International Journal of Science and Investigations*, (2012) 13.
13. A. Samimi, *International Journal of Basic and Applied science, Indonesia*, (2012) 572.
14. D. Hmamou, R. Salghi, L. Bazzi, B. Hammouti, S. Al-Deyab, L. Bammou, L. Bazzi and A. Bouyanzer, *Int. J. Electrochem. Sc.*, 7 (2012) 1303.
15. M. Migahed, A. Farag, S. Elsaed, R. Kamal, M. Mostfa and H.A. El-Bary, *Mater. Chem. Phys.*, 125 (2011) 125.
16. M. Abdullah Dar, *Industrial Lubrication and Tribology*, 63 (2011) 227.
17. H. El-Lateef, V. Abbasov, L. Aliyeva, E. Qasimov and I. Ismayilov, *Mater. Chem. Phys.*, 142 (2013) 502.
18. M. Zavareh, A.M. Sarhan, B. Razak and W. Basirun, *Ceram. Int.*, 40 (2014) 14267.
19. L. Afia, R. Salghi, L. Bammou, L. Bazzi, B. Hammouti and L. Bazzi, *Acta Metallurgica Sinica(English Letters)*, 25 (2012) 10.
20. S. Tawfik, A. Sayed and I. Aiad, *Journal of Surfactants and Detergents*, 15 (2012) 577.
21. M. Samadzadeh, S.H. Boura, M. Peikari, A. Ashrafi and M. Kasiriha, *Progress in Organic Coatings*, 70 (2011) 383.
22. H. Becerra, C. Retamoso and D. Macdonald, *Corrosion Science*, 42 (2000) 561.
23. M. Hegazy, A. El-Etre, M. El-Shafaie and K. Berry, *Journal of Molecular Liquids*, 214 (2016) 347.
24. V. Shubina, L. Gaillet, T. Chaussadent, T. Meylheuc and J. Creus, *Journal of Cleaner Production*, 112 (2016) 666.
25. R. Barker, Y. Hua and A. Neville, *International Materials Reviews*, 62 (2017) 1.
26. H. Bouazaze, F. Huet and R. Nogueira, *Electrochimica acta*, 50 (2005) 2081.
27. F. Huet and R. Nogueira, *Corrosion*, 59 (2003) 747.
28. M. Noh, *Journal of the Korean Society of Safety*, 31 (2016) 83.
29. P. de Souza, P. de Souza, J. Ferrari, J. Ferrari, I. Guedes and I. Guedes, *Anti-Corrosion Methods and Materials*, 63 (2016) 421.
30. U. Kogelschatz, *Plasma Chemistry and Plasma Processing*, 23 (2003) 1.
31. A. El-Etre and A. Ali, *Chinese Journal of Chemical Engineering*, 25 (2017) 373.